REPORT DOCUMENTATION PAGE

Form Approved OMB NO. 0704-0188

The public reporting burden for this collection of information is estimated to average 1 hour per response, including the time for reviewing instructions, searching existing data sources, gathering and maintaining the data needed, and completing and reviewing the collection of information. Send comments regarding this burden estimate or any other aspect of this collection of information, including suggesstions for reducing this burden, to Washington Headquarters Services, Directorate for Information Operations and Reports, 1215 Jefferson Davis Highway, Suite 1204, Arlington VA, 22202-4302. Respondents should be aware that notwithstanding any other provision of law, no person shall be subject to any oenalty for failing to comply with a collection of information if it does not display a currently valid OMB control number.
PLEASE DO NOT RETURN YOUR FORM TO THE ABOVE ADDRESS.

1. REPORT DATE (DD-MM-YYYY)	2. REPORT TYPE	3. DATES COVERED (From - To)
08-08-2017	Final Report	15-Aug-2015 - 16-Feb-2017

4. TITLE AND SUBTITLE

Final Report: Direct thermodynamic measurements of the energetics of information processing

5a. CONTRACT NUMBER

W911NF-15-1-0342

5b. GRANT NUMBER

5c. PROGRAM ELEMENT NUMBER

611103

6. AUTHORS

5d. PROJECT NUMBER

5e. TASK NUMBER

5f. WORK UNIT NUMBER

7. PERFORMING ORGANIZATION NAMES AND ADDRESSES

California Institute of Technology
Office of Sponsored Research
1200 E. California Blvd.
Pasadena, CA 91125 -0001

8. PERFORMING ORGANIZATION REPORT NUMBER

9. SPONSORING/MONITORING AGENCY NAME(S) AND ADDRESS (ES)

U.S. Army Research Office
P.O. Box 12211
Research Triangle Park, NC 27709-2211

10. SPONSOR/MONITOR'S ACRONYM(S)

ARO

11. SPONSOR/MONITOR'S REPORT NUMBER(S)

66800-EG-RIP.1

12. DISTRIBUTION AVAILIBILITY STATEMENT

Approved for public release; distribution is unlimited.

13. SUPPLEMENTARY NOTES

The views, opinions and/or findings contained in this report are those of the author(s) and should not contrued as an official Department of the Army position, policy or decision, unless so designated by other documentation.

14. ABSTRACT

15. SUBJECT TERMS

16. SECURITY CLASSIFICATION OF:			17. LIMITATION OF ABSTRACT	15. NUMBER OF PAGES	19a. NAME OF RESPONSIBLE PERSON
a. REPORT	b. ABSTRACT	c. THIS PAGE			Michael Roukes
UU	UU	UU	UU		19b. TELEPHONE NUMBER
					626-395-2916

Standard Form 298 (Rev 8/98)
Prescribed by ANSI Std. Z39.18

RPPR Final Report
as of 10-Aug-2017

Agency Code:

Proposal Number: 66800EGRIP **Agreement Number: W911NF-15-1-0342**

INVESTIGATOR(S):

Name: PhD Michael L. Roukes
Email: roukes@caltech.edu
Phone Number: 6263952916
Principal: Y

Organization: **California Institute of Technology**
Address: Office of Sponsored Research, Pasadena, CA 911250001
Country: USA
DUNS Number: 009584210 EIN: 951643307
Report Date: 16-May-2017 Date Received: 08-Aug-2017
Final Report for Period Beginning 15-Aug-2015 and Ending 16-Feb-2017
Title: Direct thermodynamic measurements of the energetics of information processing
Begin Performance Period: 15-Aug-2015 **End Performance Period:** 16-Feb-2017
Report Term: 0-Other
Submitted By: PhD Michael Roukes Email: roukes@caltech.edu
Phone: (626) 395-2916
Distribution Statement: 1-Approved for public release; distribution is unlimited.

STEM Degrees: **STEM Participants:**

Major Goals: The dilution refrigerator system requested will provide a low temperature environment from 20mK to 1K, to enable measurements of the thermodynamics of information processing. While physical realizations of information processing can be demonstrated in many macroscopic systems at room temperature, the thermodynamics of heat flow and entropy generation in such cases is completely overwhelmed by the environment given the minuscule nature of the signals. Carrying out experiments at ultralow temperatures and with nanoscale devices enables us to isolate the degrees-of-freedom relevant to the information storage, and to "freeze out" those that are irrelevant. This approach will enable detection of irreversible thermodynamics related to logic transitions directly in nanoscale systems.

Accomplishments: A PDF document delineating our accomplishments has been uploaded.

Training Opportunities: Nothing to Report

Results Dissemination: Nothing to Report

Honors and Awards: Nothing to Report

Protocol Activity Status:

Technology Transfer: Nothing to Report

PARTICIPANTS:

Participant Type: PD/PI
Participant: Michael L Roukes
Person Months Worked: 1.00 **Funding Support:**
Project Contribution:
International Collaboration:
International Travel:
National Academy Member: N
Other Collaborators:

RPPR Final Report
as of 10-Aug-2017

DIRECT THERMODYNAMIC MEASUREMENTS OF THE ENERGETICS OF INFORMATION PROCESSING

MATT MATHENY, OLLI SAIRA, WARREN FON, **MICHAEL ROUKES (PI)** – *CALTECH*

INTRODUCTION

The relation between thermodynamic processes out of equilibrium and information processing has been under intense investigation in the last few years. In part, this interest has been driven by the emergence of fluctuation theories (FTs) [1, 2]. It is widely assumed from various thought experiments that informational processes that do not preserve bit number (*i.e.,* non-reversible computation) must have thermodynamic repercussions [3]. The most basic of these, first stated by Landauer, is formulated for binary logic systems; specifically, on average, erasure of each 'bit' is accompanied by dissipation of $k_B \ln 2$ of energy. This dissipation should be manifested as additional heat transferred to the environmental bath into which the bit thermalizes. However, no measurement has ever been made of this heat. This project focuses upon the pursuit of such a measurement.

The proposed measurement requires two elemental units. The first is the *bit*, or the device which stores the information to be processed. The second is the *local calorimeter*, the device which measures energy along its path to being thermalized within the environment. Later in the report, we outline our progress on these experimental elements.

First, we discuss the equipment that was acquired with support from this grant. To measure the energy fluctuations of such a small energy within a reasonable (<1GHz) bandwidth, we need to "turn off" thermal conductance and heat capacity via refrigeration. Thus, the use of a dilution refrigerator with a low-millikelvin base operating temperature is essential for these measurements [4].

EXPERIMENTAL SYSTEM: PROGRESS & ACHIEVEMENTS

CRYOGEN-FREE DILUTION REFRIGERATOR SETUP

Upon approval of the award, planning for renovation of the laboratory space commenced. Simultaneously, we coordinated with the cryogen-free dilution refrigerator vendor (BlueFors, Inc.; hereafter BF) for design of the entire system. The system is a BF-LH system and consists of three major components: the cryostat/dilution unit, the cryocompressor/pulse tube, and the automatic gas handling system. The system does not require constant addition of liquid helium since it has a pulse tube refrigeration unit to precool to ~3K. The system was designed to have a line-of-sight access port from room temperature to the sample stage at room temperature should beamline protocols be necessary (such as for optical measurements of samples). The dilution refrigerator is shown in **Figure 1**. In the left picture, we show the cryostat and dilution unit. The cover plates, vacuum can, and radiation shields have been removed. This picture does not reflect recently installed wiring for the experiments. The pulse tube can be seen on top of the frame behind the setup and still line can be

Figure 1. Cryogen-Free Dilution Refrigerator System. **(Left)** Cryostat and dilution unit with vacuum can and radiation shields removed. Note that this picture was taken before the full system wiring was installed. **(Right)** Automatic gas handling system, heat exchanger for cooling water, and cryocompressor (bottom left corner).

seen going through the wall. The right picture is the other side of that wall with the automatic gas handling system, cryocompressor, and heat exchanger for the cooling water. Placing these components in a small room that is separate from the laboratory eliminates acoustic coupling to the sensitive experimental stage.

The dilution refrigerator system was delivered in November 2016 and, subsequently, installed and commissioned by the vendor in January 2017. Upon installation, He3/He4 mixture was installed from our own laboratory stock after being tested and purified (removing extraneous gases, air, and water vapor.) **Figure 2** displays the temperature as a function of time for the inaugural, installation cooldown (performed with a BlueFors engineer), and also from our most recent data. The installation cooldown was carried out without any wiring installed. Upon its installation, thermal conductance between room temperature components and the cold stage increases. If not carefully engineered, this thermal pathway can lead to significant thermal loading of the mixing chamber and cold stage. The most recent cooldown indicates a slight increase in thermal loading due the semi rigid coaxial cable, as planned, but this is completely within design parameters.

After installation and system verification, we set up the capability for measuring DC transport in superconducting weak links. The superconducting weak links first measured are Superconductor-Normal-Superconductor (SNS) junctions. These SNS junctions are mounted on a sample stage with 24 quasi-DC lines and 2 RF lines, filtered by a copper powder filter.

The front-end and back-end instrumentation for our measurements of SNS junctions consist of a programmable low noise DC power supply, a battery powered preamp, and a 24-bit digital multimeter.

In addition to the aforementioned DC measurement capabilities, we also installed 4 RF coaxial lines in one cryostat port to enable RF measurements of NEMS devices. These coaxial lines are fabricated using UT-034 Be-Cu semi-rigid cable and SMA connectors; this special alloy provides reasonably low Ohmic losses but far better thermal isolation than elemental (e.g., Cu) conductors. With both DC and RF lines installed, we have demonstrated achievement of an 8mK base temperature.

TEMPERATURE MEASUREMENTS WITH SUPERCONDUCTING WEAK LINKS

As mentioned, our planned measurements involve interposing a local, isolated, ultrasensitive calorimeter in the thermalization pathway between the *logic bit* and the *environment*. With an ideal hierarchy of scattering rates amongst the microscopic mechanisms mediating energy transport, the isolated calorimeter can enable direct and quantitative observation of the bit's thermalization processes. The requisite "isolated calorimeter" has two principal elements: the local *phonon cavity* (realized as a mesoscopic dielectric element that is strongly coupled to the bit, and weakly coupled to the environment) and a fast and ultrasensitive local *thermometer* (which permits monitoring the energetic state of the relevant degrees-of-freedom within the isolated calorimeter.) In our original proposal, we have discussed measurements permitting the characterization of the thermometer element. In our first experiments using the new cryogenic system, we have characterized a potential thermometer embodiment, comprising a superconducting weak link whose superconducting-to-normal transition temperature is much lower than that of bulk superconductor values.

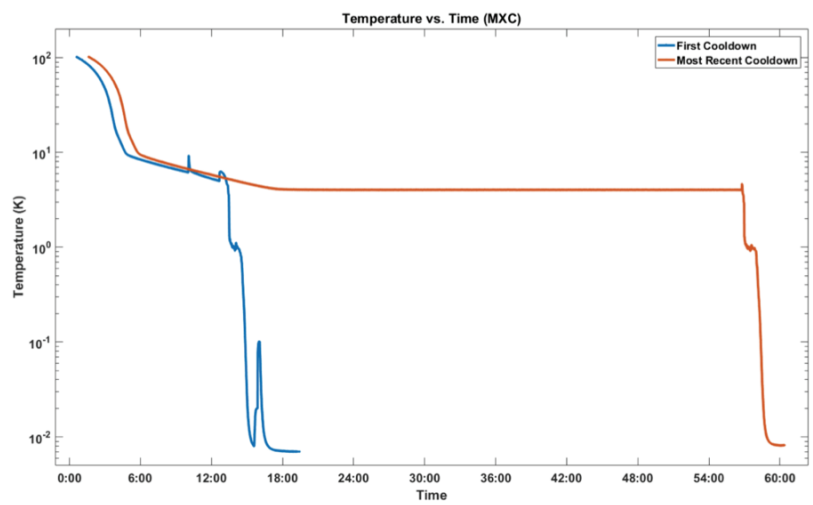

Figure 2. System temperature *v.* time on newly-installed dilution refrigerator. The blue curve indicates the first cooldown performed with the equipment vendor's engineer on-site. The 'bump' at low temperatures is adjustment of parameters performed by the engineer. The blue curve has no wiring. The orange curve is the most recent cooldown. Between 18:00 and 56:00 hours a device was being tested at 3K. Removing this 'dead time' indicates that to achieve cooldown with wiring requires no additional time. Red trace is from a subsequent cool-down including stage modifications; low thermal conductance coaxial cables have been included with no deleterious effect upon base temperature.

In **Figure 3** we display micrographs of weak links and their I,V-curves as a function of temperature. We have characterized two different types of superconducting weak links. The upper left panel of Figure 3 displays a micrograph of a

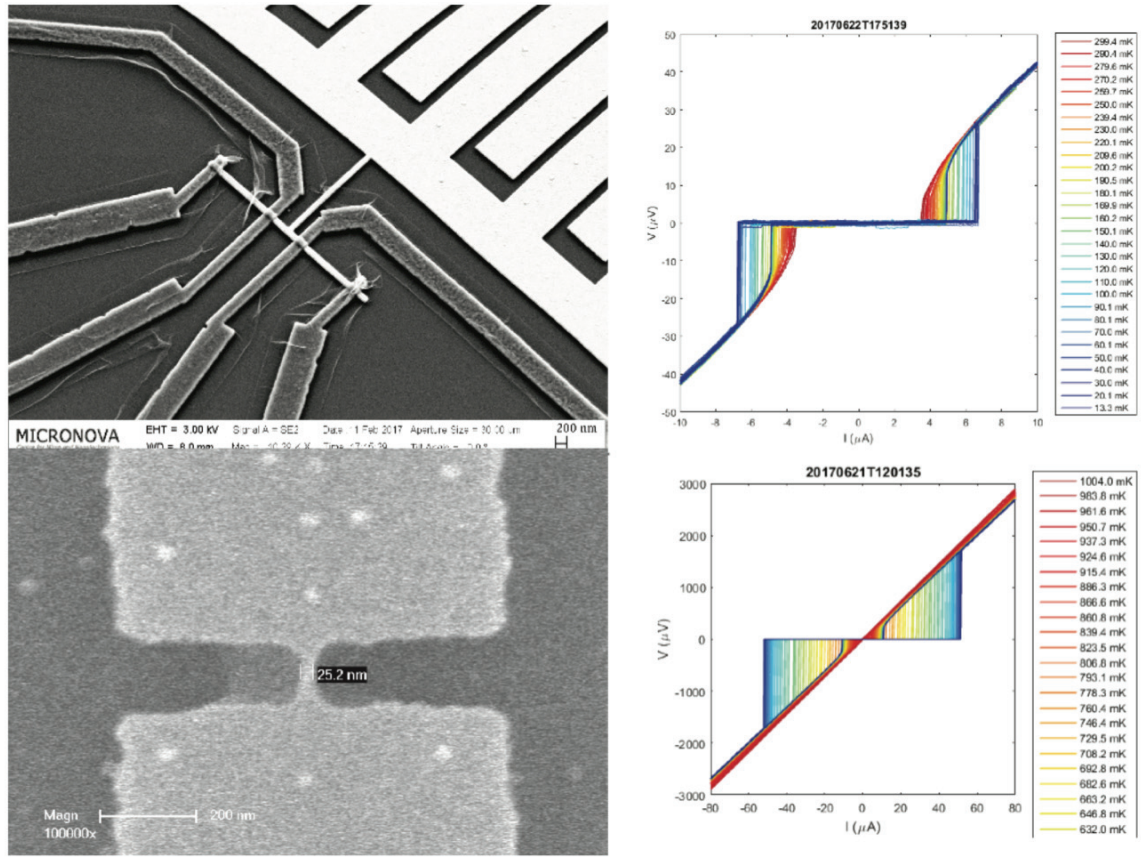

Figure 3. DC transport of Superconducting weak links. (Upper left) SNS weak link. The bright region is gold, and the dark lines are aluminum. **(Upper right)** The IV-curve of the SNS junction where the color indicates temperature. **(Lower left)** Molybdenum Dayem bridge with 25nm width. **(Lower Right)** The IV-curve of the Dayem bridge Josephson Junction where the color indicates temperature.

superconductor/normal-metal/superconductor (SNS) junction formed from an Aluminum-Gold-Aluminum tri-layer; the weak link's dimensions are 1μm×0.2μm (*l*×*w*). The second micrograph is of a Dayem bridge, *i.e.*, a narrow constriction within a superconducting lead. The device depicted in the lower left corner of Figure 3 is formed from a Molybdenum thin film, with a weak link formed by a constriction with dimensions of approximately 0.16μm×0.025μm (*l*×*w*). These devices both operate in the underdamped regime, which results in the prominent hysteresis in their respective I,V-curves (Figure 3; upper right and lower right.) In both of these figures we display a family of I,V-curves corresponding to different temperatures, and color-coded according to their respective legends.

These two thermometers have complementary ranges of application. The SNS junction has peak temperature sensitivity between 50mK and 300mK, while the Mo Dayem bridge exhibits peak sensitivity between 250mK and 850mK. In Figure 4, we show the temperature dependence of the specific current at which the junctions switch from the superconducting to normal state and, vice-versa. We term the transitions *to* and *from* the superconducting state the 'switching' and 'retrapping' currents, respectively. The hysteresis -- that is, the difference between the switching and retrapping branches – grows as the device is cooled to lower temperatures.

The next step in our experimental program is to fabricate each of these local thermometers directly upon a phonon cavity, embodied as a suspended dielectric platform. This will permit realization of the desired, highly sensitive calorimeters.

Developing ideal and appropriate measurement protocols for measuring ultralow energy transport are complex [5]. In this vein, much of the latter half year of our system assembly effort has been spent reducing sources of noise in the experimental setup. The first measurement of the SNS junction saturated at a temperature of ~200mK and showed no hysteresis. These junctions are fabricated by our collaborators in Professor Jukka Pekola's group in Helsinki, and were characterized there before shipment to Caltech. Our latest data from this same device, obtained after improvements to the measurement system, are shown at the top of Figure 4. The much lower saturation temperature of ~50mK is readily evident and is now in agreement with the Pekola's group results with these SNS junctions. This validates our low noise measurements and indicates that our electron temperature in these devices is currently below ~50mK. In future work, we will fabricate and measure longer devices fabricated as Superconductor-*Semiconductor*-Superconductor junctions. The low electron densities available in high quality semiconductor heterostructures will extend the range of optimal temperature sensitivity down to the 10mK temperature regime. This extended range is critical for our planned experiments on energy transport.

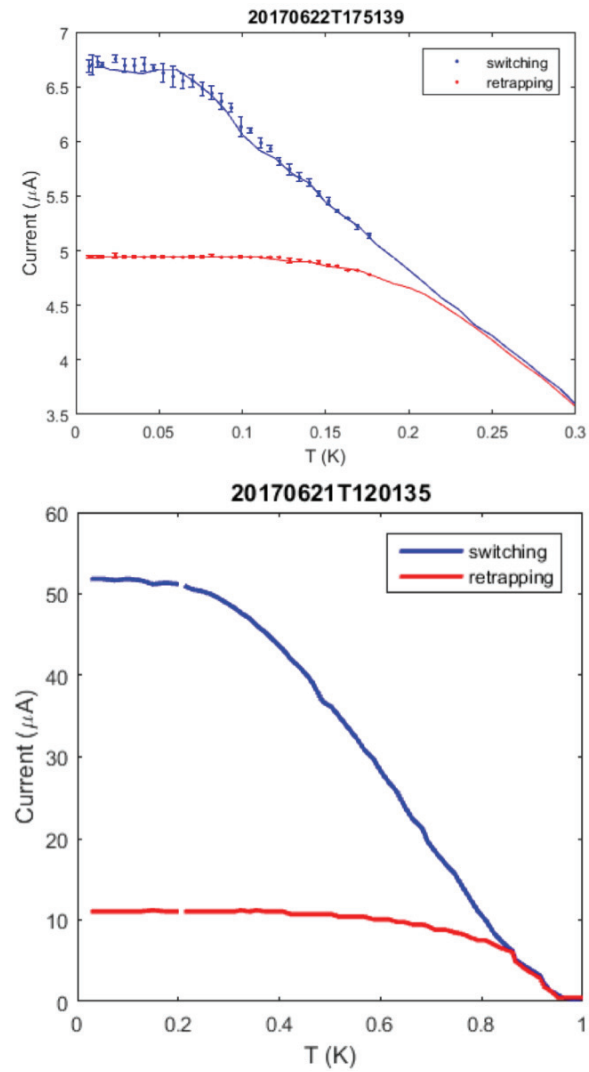

Figure 4. Switching and Retrapping currents of two superconducting weak links. (Top) Al-Au-Al SNS junction. **(Bottom)** Molybdenum Dayem bridge. The temperature range of the SNS junction spans a lower range than the Mo Dayem bridge.

MEASUREMENTS OF NANOELECTROMECHANICAL SYSTEMS FROM 8MK TO 300K

One of the experiment embodiments we are pursuing in this work consists of a nanomechanical switch coupled to an ultrasensitive calorimeter. We are currently perfecting long NEMS beams for operation as a two-state nanomechanical logic gate (through beam buckling). Here, we discuss our initial measurements on nanomechanical devices which patterned and measured just prior to the

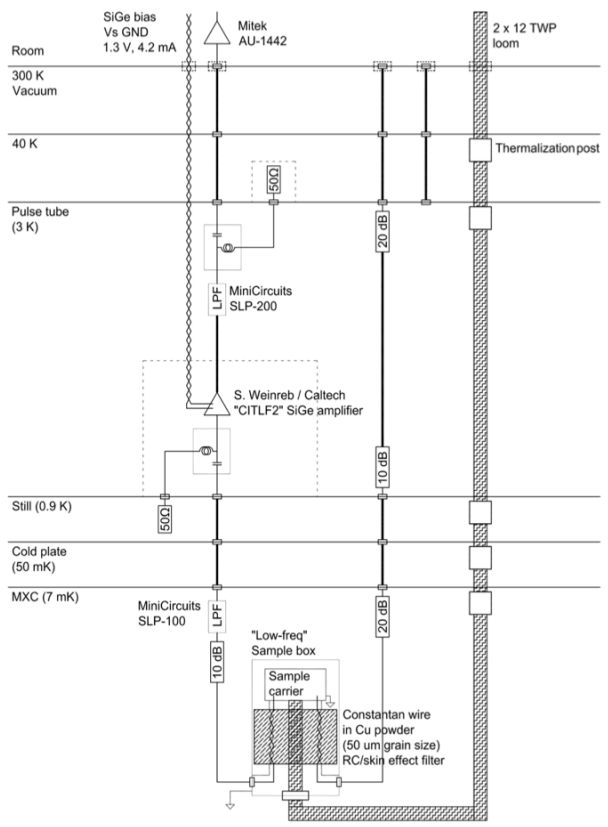

Figure 5. Experimental setup for measurement of NEMS devices.

writing of this final DURIP report. These initial data directly demonstrate our ability to drive and detect nanomechanical motion at ultralow temperatures.

In addition, these measurements also provide a first indication of the scattering rates for phonon modes operative in NEMS when cooled to low temperatures. Together the multiple modes of the mechanical resonators themselves constitute a phonon cavity, and these can act as local heat baths for our calorimeters. Accordingly, their intermode scattering rates will determine relevant thermal time constants. As shown by our data and that from other labs, these scattering rates decrease with decreasing temperature. This also indicates, indirectly, that their heat capacities also decrease with temperature, as expected. Scattering centers that can be thermally excited at ultralow temperatures are known to cause dissipation and dephasing in mechanical resonators. Our data provides evidence that the strength of these scattering processes continue to decrease below 100mK.

Our measurements on NEMS are obtained by exciting and observing the vibrational modes of piezoelectric (Aluminum Nitride) nanomembranes from room temperature down to ultralow temperatures. The piezoelectric device topology permits direct conversion between the electric field and the elastic field. Our two-port electromechanical resonator can be modeled by an equivalent series-RLC circuit. The device output is amplified by a cryogenically cooled SiGe heterostructure bipolar transistor (HBT) amplifier, with an input impedance of 50Ω and a noise temperature of ~2K. We inserted a 10dB attenuator between the sample and the amplifier to attenuate backaction noise from the amplifier input into the device; this enables our first measurements keeping the electron temperature in the device low, although it significantly degrades the noise figure in this preliminary study. In future set-ups we will replace this attenuator with a cryogenically cooled non-reciprocal element that will shunt the amplifier's backaction noise to a cold load while providing low-loss transmission of the NEMS ouput to the amplifier. A schematic representation of the present setup is depicted in **Figure 5**.

The device we measured is an ultrathin square piezoelectric membrane with a cross-sectional dimenion of 40μm, shown in **Figure 6**, left panel. Although the extent of the membrane is not readily apparent in the micrograph, its position is indicated by the black dots within the middle of the device. These are tiny release holes etched into the material stack, to permit free suspension of the membrane after exposure to a specific etchant. The fundamental resonance of the out-of-plane

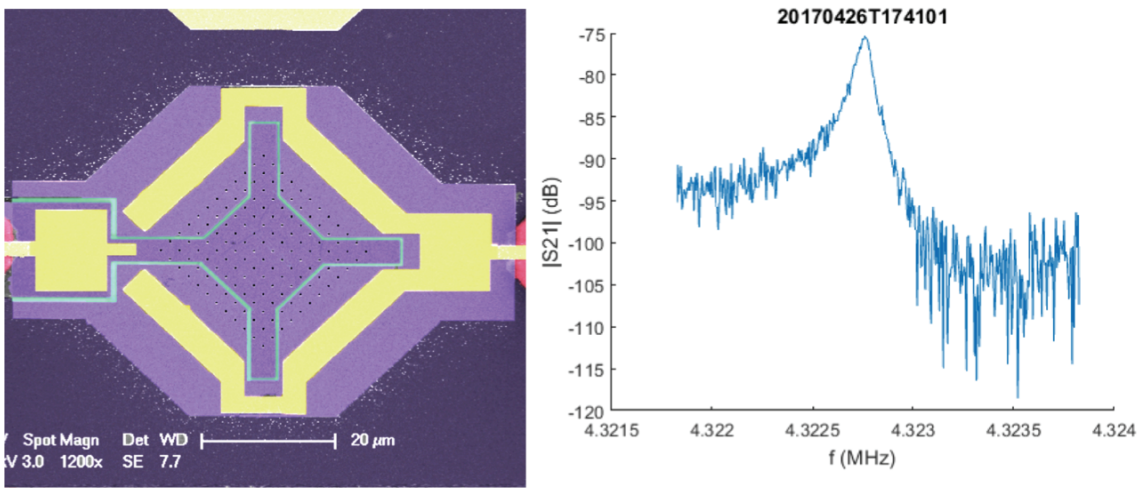

Figure 6. Nanomembrane-based NEMS Device. **(Left)** Membrane is cut out using release holes in the purple layer. Electrodes are cut between input and output by the green cut out. **(Right)** Resonant response of fundamental membrane mode.

"drumhead" mode is evident in the plot of transmitted power *v.* excitation frequency, shown in the right panel of **Figure 6**. We find that this mode typically has a very high quality factor, ranging between 100,000 and 200,000 – the precise value is dependent on the specific device measured. **Figure 7** provides representative data from one device, showing the evolution of fundamental-mode frequency and quality factor with decreasing temperature.

Piezoelectric NEMS permit ultralow power measurements because of the direct electron-phonon coupling of piezoelectric materials. In our devices, we employ Mo electrodes of above and below the piezoelectric layer. Our measurements show that these become superconducting at T_c~900mK. This circumvents electron heating in the actuation electrodes, which enables measurements at mK temperatures. In **Figure 8, left panel**, we show the transmitted power v. excitation frequency swept from 1MHz to 200MHz. The wideband sweep shows approximately 26 modes in this frequency range. We note that our copper powder filters likely reduce the transmitted power above 100MHz. In addition, the wiring likely has stray capacitance which dominates the signal above 100MHz. Thus, it turns out to be more challenging to find modes above 100MHz using the current setup. Our next-gen setup will be optimized for higher frequency measurements, and even higher frequency modes should be observable.

In **Figure 8, right panel,** we show a plot of quality factor against frequency for the ~26 modes. To our knowledge, tracking such a large number of modes at low temperature has never been

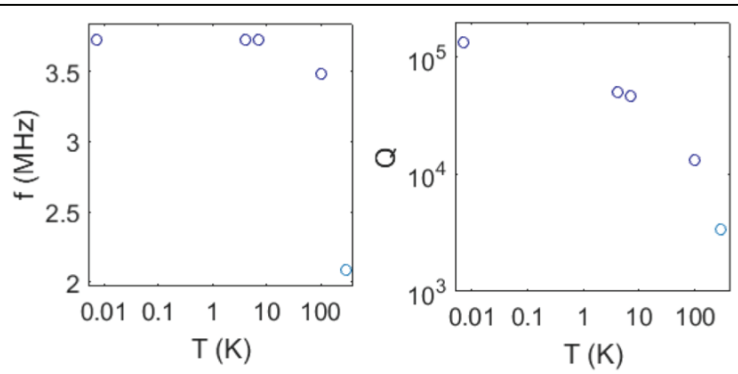

Figure 7. Frequency and Quality Factor of the nanomembrane fundamental mode as a function of temperature. The frequency saturates around 4K but the quality factor continues to increase.

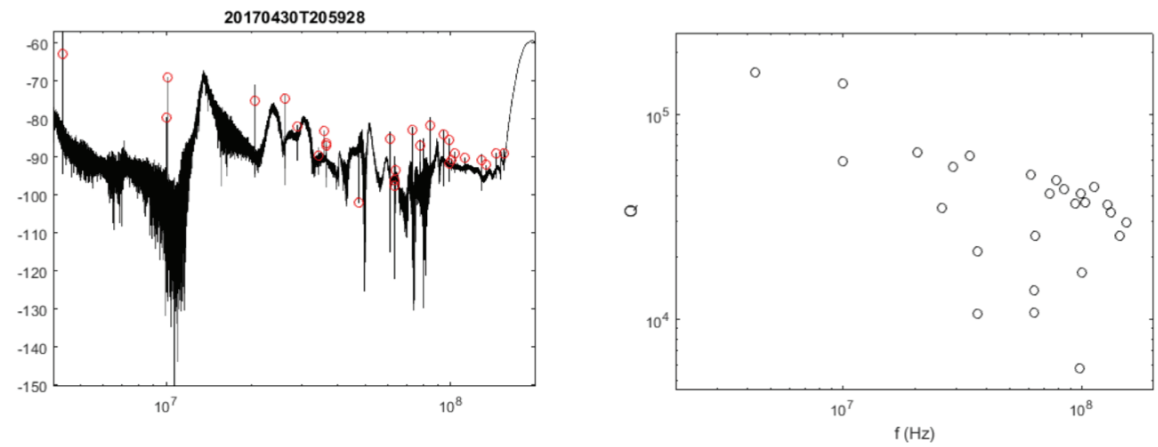

Figure 8. Frequency response of cryogenically-cooled Nanomembrane device. (Left) Wide frequency sweep of driven nanomembrane response. Resonance are indicated with red circles. Modes above 100MHz are difficult to find due to parasitic capacitance and low temperature electronic filters. **(Right)** Scatter plot of the mode frequencies against quality factors.

performed before. The data is consistent with internal relaxation ($Q \propto 1/f$), and does not appear to reflect radiation losses at the boundaries [6]. These 30 modes are all out-of-plane drumhead-like modes of the membrane. These modes should, in fact, constitute the majority of the phonon heat capacity of the membrane. As this measurement is done using a membrane that is fully clamped around its periphery, it provides a upper bound on the phonon thermal conductivity to the environment. Supporting the membrane to the substrate with very narrow legs at its corners will provide much lower thermal coupling to the environment [5].

Figure 7 shows that, below about 10K, the resonant frequency of the device saturates at higher values. This likely originates from temperature-induced stress arising from differential thermal contractions between the membrane and the underlying silicon to which it is clamped. Thermal contraction of silicon saturates at around 10K. Notice that the quality factor of the resonator does not saturate in this temperature range but continues to increase. This indicates that the dissipation is changing and not just the frequency-to-relaxation rate as indicated by quality factor. We are exploring the dissipation mechanisms operative at lower

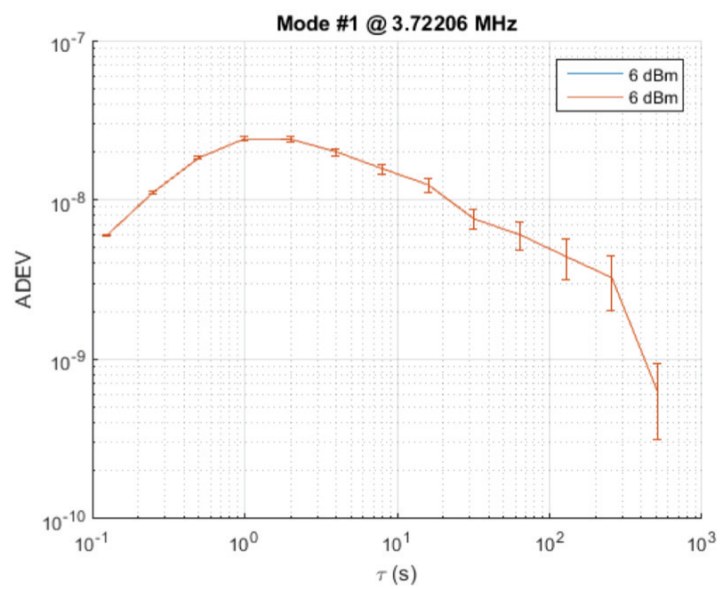

Figure 9. Allan Deviation as a function of integration time.

temperatures. We note that although quasi-particle densities within the Mo superconductors become exponentially suppressed below 100mK, we do not see large changes in quality factor below this regime.

We also include data which indicates the dephasing of the system. We measured the transmitted phase as a function of time and calculated the Allan variance at times ~30min. **Figure 9** shows the Allan Deviation for the first resonant mode at 8mK. For long integration times, the Allan Deviation is below 10^{-9}. Equivalent room temperature measurements under ideal conditions typically yield a value of ~10^{-7}. This indicates that significantly lower dephasing is occurring in the system at ultralow temperatures. It indicates that low-energy degrees-of-freedom that directly interact with the phonon cavity are frozen out at low temperatures, which is favorable for the experiments we are now embarking upon.

SUMMARY

In this final report, we have discussed our successful assembly of the ultralow temperature measurement system we have assembled with DURIP funding to observe, directly, the energetic changes in nanoscale information engines. Our first work with this system to explore superconducting weak link based thermometers shows their high sensitivity down to 50mK. This verifies that our dilution refrigerator and the electronic instrumentation we have assembled are working ideally. Weak links with even lower effective gaps will be pursued in the future.

We also have shown that we can measure coherent dynamics of phonon cavities across the working range of temperatures. The quality factor versus mode trend we observed indicates we are limited by boundary scattering. The quality factor versus temperature indicates this as well, although further reductions are expected with weak anchoring to the substrate. Both dephasing and dissipation was shown to decrease substantially at these ultralow temperatures, for which further measurements of improved devices should reveal very long phonon relaxation times.

REFERENCES

1. Jarzynski, C., *Nonequilibrium equality for free energy differences.* Physical Review Letters, 1997. **78**(14): p. 2690.

2. Crooks, G.E., *Entropy production fluctuation theorem and the nonequilibrium work relation for free energy differences.* Physical Review E, 1999. **60**(3): p. 2721.

3. Landauer, R., *Irreversibility and heat generation in the computing process.* IBM journal of research and development, 1961. **5**(3): p. 183-191.

4. Roukes, M., *Yoctocalorimetry: phonon counting in nanostructures.* Physica B: Condensed Matter, 1999. **263**: p. 1-15.

5. Schwab, K., Henriksen, E.A., Worlock, J.M., and Roukes, M.L., *Measurement of the quantum of thermal conductance.* Nature, 2000. **404**(6781): p. 974-977.

6. Ghadimi, A.H., Wilson, D.J., and Kippenberg, T.J., *Radiation and internal loss engineering of high-stress silicon nitride nanobeams.* Nano Letters, 2017.